QCM-D and NanoTweezer Measurements to Characterize the Effect of Soil Cellulase on the Deposition of PEG-coated TiO_2 Nanoparticles in Model Subsurface Environments†

Submitted to:
Environmental Science: Nano
2018

M.O. AKANBI[A], L.M. HERNANDEZ[A], M. H. MOBAROK[B], J.G.C VEINOT[B], & N. TUFENKJI[A]*

[a] *Department of Chemical Engineering, McGill University, Montreal, Quebec, Canada.*
[b] *Department of Chemistry, University of Alberta, Edmonton, Canada.*
**Corresponding Author. Phone: (514) 398-2999; Fax: (514) 398-6678; E-mail: nathalie.tufenkji@mcgill.ca*
† Electronic Supplementary Information (ESI) available

Abstract

Upon release to the environment, engineered nanoparticles (ENPs) undergo several chemical, physical and biological transformations that may affect their fate, transport, and bioavailability. The impact of ENP transformations (e.g., coating with natural organic matter or heteroaggregation with natural colloids) on ENP fate and transport has been systematically examined; however, the influence of soil enzymes that are ubiquitous in soils has not been considered. In this study, we examined the effect of a model extracellular soil enzyme (cellulase) – either free in an artificial porewater or adsorbed on a model aquifer grain (silica) surface – on the deposition kinetics of polyethylene glycol-coated titanium dioxide nanoparticles (PEG-nTiO_2). A quartz crystal microbalance with dissipation monitoring (QCM-D) was used to study the interaction of PEG-nTiO_2 with bare and cellulase-coated silica surfaces as well as in the presence of free cellulase over a range of sodium chloride concentrations. Significant reduction in PEG-nTiO_2 deposition rates was observed in the presence of cellulase indicative of strong repulsive interactions between the nanoparticles and the layer of cellulase adsorbed on the silica surface. QCM-D observations were supported by measurements of the PEG-nTiO_2-surface interaction energies using an optical NanoTweezer apparatus revealing more repulsive particle-surface interaction energies for the cellulase-coated silica. QCM-D measurements also indicated formation of more viscoelastic films in the presence of cellulase compared to bare silica except at the lowest ionic strength (IS) studied (10 mM NaCl). Overall, this work shows the potential for increased mobility of ENPs in subsurface environments in the presence of extracellular soil enzymes, motivating the need for further studies on the fate and behaviour of ENPs in the presence of these ubiquitous biomolecules.

Keywords: optical tweezer, quartz crystal microbalance, soil enzyme, nanoparticle transport, environmental risk

1. Introduction

Nanoscale titanium dioxide particles ($nTiO_2$) are used in the manufacture of consumer products such as cosmetics and paints for their ability to absorb UV radiation.[1] Also, $nTiO_2$ possesses photocatalytic properties which make it suitable for industrial applications such as self-cleaning surfaces.[2, 3] The increased use and production of $nTiO_2$ increases the likelihood of its release into the environment. Studies have predicted that $nTiO_2$ particles are likely to be found in concentrations up to 21 ng L^{-1} in surface waters, 4 μg L^{-1} in sewage treatment effluents and 89 μg kg^{-1} in sludge treated soils.[1, 4] In particular, Kaegi et al. demonstrated the release of $nTiO_2$ from the exterior facade of buildings into the aquatic environment at concentrations as high as 600 μg L^{-1}.[5]

The fate and behaviour of ENPs, such as $nTiO_2$, in aquatic environments are of growing interest due to their potential environmental and public health risks.[6] Upon release into the environment, ENPs undergo several chemical, physical and biological transformations that may affect their environmental fate, transport, and bioavailability.[7-9] In natural soils and groundwater, particle-specific properties such as size, shape, chemical composition, surface charge and coating, and porewater chemistry (e.g., pH, ionic strength, ionic composition, and natural organic matter content) determine the aggregation and deposition behaviour of these particles.[10-12] In these environments, naturally occurring particles (e.g., clays, silicates) and organic macromolecules are pervasive;[13, 14] thus, there is a strong likelihood for interaction of ENPs with these particles and macromolecules. Several researchers have studied the adsorption of natural organic matter such as humic and fulvic acids on $nTiO_2$[15-18] showing their effect on particle stability. The effect of natural colloids such as silicates and phosphates has also been examined.[19, 20] Although proteins make up a significant fraction (approximately 30% by weight[21, 22]) of soil macromolecules, little is known about their potential influence on ENP properties and environmental behaviour.

Soil microorganisms such as bacteria, fungi and protozoa produce and secrete a range of extracellular enzymes, including oxidases, phosphatases, proteases and cellulases.[23-25] These proteins may subsequently be adsorbed onto the surfaces of sediment or aquifer grains forming surface heterogeneities that may influence particle deposition and retention.[26] Proteins may also remain in the porewater where they can interact with suspended ENPs, and form a protein corona, thereby influencing ENP aggregation and deposition behaviour.[27-29] Few studies have examined the adsorption of human serum proteins onto the surface of $nTiO_2$ and characterized the protein corona that is composed of a hard core of strongly bound proteins and a soft outer layer of diffusing molecules.[30-32] However, little is known about the interaction of environmental proteins with ENPs and its potential impact on the fate of ENPs.

Cellulases are a group of hydrolytic enzymes produced and secreted by soil microbes to decompose cellulose into oligosaccharides, cellobiose and glucose.[33] In order to hydrolyze and metabolize cellulose,

microorganisms secrete cellulases that are either free or cell-surface bound.[33, 34] The molecular mass of cellulases is dependent on their source and can span a wide range. Molecular weight of fungal cellulases ranges from 30 kDa to 250 kDa.[35] Cellulases are modular proteins that contain noncatalytic carbohydrate-binding modules and/or other functionally known or unknown modules that may be located at the N- or C-terminus of a catalytic module.[33, 36] They are known to sorb onto the surface of clays and humics in soil environments.[34, 37] Also, studies have shown that cellulases can be immobilized onto silica.[38, 39] *Aspergillus* spp. fungi which are highly efficient producers of extracellular enzymes are present in nearly all soils and other natural habitats.[40] The protein secretion level observed in *Aspergillus niger* is reported to be up to 20 g/L.[41] Therefore, *Aspergillus niger* cellulase was used as a model extracellular enzyme for the purpose of this study.

The objective of this study was to investigate the influence of a common extracellular soil enzyme (cellulase), either suspended (free) in an artificial porewater or adsorbed on a model aquifer grain (silica) surface, on the deposition kinetics of polyethylene-glycol (PEG)-coated $nTiO_2$ (PEG-$nTiO_2$). Cellulases are a group of hydrolytic enzymes produced and secreted by soil microbes to decompose cellulose. A quartz crystal microbalance with dissipation monitoring (QCM-D) was used to study the interaction of PEG-$nTiO_2$ with a bare silica surface, silica pre-coated with cellulase and in the presence of free cellulase over a range of NaCl concentrations. The deposition kinetics of PEG-$nTiO_2$ onto the bare and cellulase-coated silica surfaces are compared and the potential influence of cellulase on the fate and behaviour of PEG-$nTiO_2$ in aquatic environments is discussed. To support interpretation of the QCM-D measurements, a NanoTweezer apparatus was used to characterize nanoparticle-surface interaction energies in the presence and absence of cellulase.

2. Materials and Methods

2.1 Preparation of Nanoparticle Suspensions

21 nm PEG-$nTiO_2$ were synthesized using a modified catalytic chain transfer and thiol-ene chemistry as detailed in the Supplementary Information.[42] The scheme for the surface modification of the $nTiO_2$ is shown in Figure S1 of the Supplementary Information.

A stock suspension of 20 g/L PEG-$nTiO_2$ (21 nm) was prepared by suspending the PEG-$nTiO_2$ in vacuum filtered (0.22 μm cellulose cetate filter, Fisher) deionized (DI) water and kept refrigerated at 4 °C in the dark.[43] Prior to each experiment, suspensions of PEG-$nTiO_2$ were prepared by diluting the stock suspension in NaCl solutions at different salt concentrations (IS = 1-300 mM), mixed using a vortex mixer set at high speed and the pH adjusted to 5.5±0.1 using NaOH. Analytical grade chemicals (Fisher) were used.

2.2 Preparation of Cellulase Suspension

A stock suspension of 1000 ppm cellulase was prepared by dissolving powdered cellulase (*Aspergillus niger*, ≥0.3 units/mg solid, Sigma Aldrich) in vacuum filtered (0.22 μm cellulose acetate filter, Fisher) DI water and kept refrigerated at 4 °C in the dark overnight. Prior to each experiment, a working suspension of cellulase (150 ppm) was prepared by diluting the stock suspension in NaCl solutions (artificial porewaters) at different salt concentrations (IS 1-300 mM), mixed using a vortex mixer set at high speed and the pH adjusted to 5.5±0.1 using NaOH. The concentration of cellulase was selected to correspond to estimated levels in natural soils. [41, 44, 45]

2.3 Nanoparticle Characterization

Dynamic light scattering (DLS; Zetasizer Nano ZS, Malvern) was used to measure the hydrodynamic diameters of the PEG-$nTiO_2$ suspended in the artificial porewaters. These measurements were done using three different samples. Laser Doppler velocimetry (Zetasizer Nano ZS; Malvern) was used to characterize the electrophoretic mobility (EPM) of the nanoparticles within the range of IS tested. Triplicate measurements were made using a dip cell at 20 °C ± 0.2 °C. An electric field of 4.9 ± 0.1 V m^{-1} was applied. Measured EPMs were converted to zeta potentials using the Smoluchowski equation.[46]

Transmission electron microscopy (TEM) was used to image and measure the size of the PEG-$nTiO_2$ nanoparticles suspended in DI water. 10 μL drop of PEG-$nTiO_2$ suspension was placed on a glow-discharged carbon coated copper grid and allowed to dry for about 5 min. The grid was then washed thrice by placing on drops of DI water for 10 s and the excess water removed by touching the grid to a filter paper. The grid was then negative stained using 2% uranyl acetate and the excess stain removed after 10 s by touching the edge of the grid to a filter paper. The grid was subsequently dried at room

temperature before loading into the TEM specimen holder. All samples were examined using a FEI Tecnai 120 kV TEM and images were captured using a Gatan Ultrascan 4000 4k × 4k CCD camera. Image J was used to obtain the particle size distribution by measuring a total of 350 particles from micrographs obtained from 3 different TEM grids.

2.4 Quartz Crystal Microbalance with Dissipation Monitoring (QCM-D)

The deposition kinetics of PEG-nTiO_2 onto bare and cellulase-coated silica were measured using a Q-Sense AB E4 unit with 5 MHz AT-cut crystals having a silica-coated surface (QSX303, Q-Sense). Injected suspensions flow parallel to the flat SiO_2 surface. Nanoparticle deposition experiments were conducted in triplicate with changes in the frequency (Δf) and energy dissipation (ΔD) monitored simultaneously. For all experiments conducted, the flow rate of the background solutions and nanoparticle suspensions was maintained constant at 50 μL min^{-1} and the temperature inside the flow modules was stabilized at 20.00 ± 0.02 °C.

Prior to each QCM-D experiment, the crystals were cleaned by soaking in 2% Hellmanex overnight, rinsed with DI, dried under nitrogen gas and then exposed to UV/ozone treatment for 20 min. For each experiment, a peristaltic pump (Reglo-Digital IPC-N 4; Ismatec) was first used to inject the background particle-free artificial porewater (electrolyte) solution until a stable baseline was obtained. Next, the nanoparticle suspension in the same porewater solution was injected into the measurement chamber for 20 min. Finally, the porewater solution was flowed through for 15 min. As PEG-nTiO_2 deposits on the bare or cellulase-coated silica surface, the increase in mass per unit area (Δm_f) of the crystal surface can be determined from the measured shift in the oscillating frequencies of the crystal using the Sauerbrey relationship: [47]

$$\Delta m_f = -C\frac{1}{n}\Delta f_n \qquad (1)$$

where C=17.7 ng cm^{-2} Hz^{-1} is the mass sensitivity constant for a 5 MHz quartz crystal, n is the overtone number (1, 3, 5, 7, 9) and Δf_n is the shift in resonance frequency at overtone number *n* (Hz).

When the Sauerbrey relation is valid, the rate at which mass is deposited on the silica surface is given by the rate at which the frequency shift changes with time:

$$r_d = -f_{n_{slope}} = -\frac{d\Delta f_n}{dt} \qquad (2) \quad \text{(Hz } min^{-1}\text{)}$$

Energy dissipation of the oscillating crystal was measured as the exponentially dissipated sinusoidal voltage signal over the crystal as a result of switching off the applied voltage to the piezoelectric oscillator. The D factor was acquired from the Q-Sense software using the equation:

$$D = \frac{E_{dissipated}}{2\pi E_{stored}} \qquad (3)$$

where $E_{dissipated}$ is the energy lost during one oscillation cycle and E_{stored} is the total energy stored in the oscillator. The D factor provides information on the viscoelastic properties of the deposited layer.

After each experiment, the crystals, chambers and tubing were cleaned with 20 mL of 10 mM NaOH, 10 mL of DI water, 20 mL of 2% Hellmanex (Fisher Scientific) and 30 mL of DI.

In this study, deposition rates of PEG-nTiO_2 suspended in different concentrations of NaCl at the different conditions studied were obtained from the initial changes in frequency shifts (Δf_n) as a function of time (eq. 2). The normalized frequency shifts for the third overtone (*i.e.,* $\Delta f_{(3)}$) were used to calculate the nanoparticle deposition rates. Also, dissipative energy losses (ΔD) at each experimental condition are presented as the ratio $-\Delta D_{(3)}/\Delta f_{(3)}$. This ratio can provide insight into the stiffness of the particle-surface bond,[48] particle size[49, 50] and conformation of stabilizing polymeric coatings.[51]

2.5 Pre-coating the Silica Surface with Cellulase

For deposition experiments conducted on surfaces pre-coated with *A. niger* cellulase, the background artificial porewater solution was flowed across the bare silica surface until a stable baseline was obtained. Next, 1 mL of enzyme suspension (150 ppm) prepared in the porewater solution was flowed across the crystal surface to deposit cellulase molecules onto the silica. Finally, the formed cellulase layer was rinsed with the background artificial porewater solution to remove loosely bound cellulase molecules until a stable baseline was obtained.

2.6 NanoTweezer Surface Measurements

Interactions of PEG-nTiO_2 particles with bare and cellulase-coated silica were measured using the NanoTweezer surface equipment (Optofluidics, Philadelphia, PA). This equipment operates on a waveguide-based method inspired by the Total Internal Reflection Microscopy (TIRM) technique, in which light (confined in two dimensions) interacts with a particle attracting it towards a surface.[52] An evanescent field is generated at the interface between the surface and the particles and the particles will scatter an intensity of light dependent on the position of the particles within the evanescent field.[52] The amount of scattered light is measured and used to map a potential well of the interaction. The

TIRM technique has limitations when used to measure smaller particles, as the signal-to-noise ratio decreases with the size of the particle trapped. The NanoTweezer overcomes these limitations by confining in two dimensions the light source and the particles in a waveguide structure thereby increasing the signal-to-noise ratio.[52, 53] The NanoTweezer measures the intensity of the scattered light and correlates it (using confined Brownian motion) to the interaction between the particle and the surface. The NanoTweezer software uses a Boltzmann inversion (derived from several force and energy balances)[52-54] to calculate the equilibrium state (as the most probable state) and compare all other states to the equilibrium thereby obtaining a potential energy map. It is known that the primary component of the particle-surface interaction is due to the overlapping of electrical double layers; therefore, according to the DLVO theory, we have a screened electrostatic interaction, that has the form:

$$\frac{U}{k_b T} = A e^{\frac{-z}{\lambda_D}} \qquad (4)$$

where U is the interaction energy, k_b is the Boltzmann constant, T is the absolute temperature, z is the distance between the nanoparticle and the surface, λ_D is the Debye screening length, and A is a parameter related to steric and electrostatic interactions.[52]

In the NanoTweezer (Figure S2), the uniform laminar flow of suspensions through a silica chip is controlled using an in-line flow sensor and a PID feed control loop. A laser is aligned to a waveguide in which it is confined in two dimensions. Particles passing by the waveguide are trapped by the evanescent field and moved along the waveguide by optical forces.[52] The scattering of light generated by this interaction is recorded with a CMOS camera.

To measure particle-surface interactions of PEG-nTiO_2 with cellulase-coated silica, 0.12 mL of a 150 ppm cellulase suspension was initially flowed through the chip at 4 μL min^{-1} for 30 min. Videos were taken during flow of free cellulase in the chip to confirm that cellulase molecules do not scatter significant light themselves. Next, 60 μL of electrolyte was flowed through at 4 μL min^{-1} for 15 min to remove loosely bound cellulase, and once again, videos were recorded as an additional control treatment. To measure the interaction between the silica surface (bare and cellulase-coated) and the particles, the particle suspension was flowed at 0.1 μL min^{-1} through the chip and the laser power was adjusted to capture the particles. The laser power required is dependent on the IS of the sample (5–12.5 mV for the IS range tested). The salt concentrations used in the NanoTweezer experiments were much lower (0.5-1.5 mM NaCl) than those used in the QCM-D experiments. Attempts to measure particle-surface interaction energies at higher NaCl concentrations were unsuccessful due to rapid particle deposition onto the waveguide surface in the presence of weak repulsive interactions. Thus, one limitation of the NanoTweezer is that measurements are restricted to conditions where repulsive interactions dominate. Sixty videos of each sample were taken, tracking at least 60 particles per experiment and a minimum of 3000 measurements/particle was applied.

The raw data collected by the NanoTweezer are in the form of high speed images which in sequence form a high-resolution video in which the movement of the particles can be observed. With the information obtained from the videos recorded, parameters A and λ_D in eq. 4 were calculated for each particle-surface combination. These parameters were calculated with the NanoTweezer software by using a Boltzmann inversion that calculates the energy equilibrium states of each tracked particle, and then compares these states to all other energy states; this forms an energy map for each specific tracked particle. The average of all the particles tracked in the same experiment forms the energy map that describes the particle interaction at the specific conditions of the experiment.

3. Results

3.1 Nanoparticle characterization

Size and EPM measurements of PEG-nTiO_2 suspended in different NaCl solutions at pH 5.5±0.1 were performed prior to each QCM-D experiment. EPM measurements were subsequently converted to zeta potentials. From the data presented in Figure 1, it can be seen that in the presence and absence of cellulase, increase in the IS results in a decrease in the absolute zeta potentials due to compression of the electrical double layer.[55] Also, we observed that at the same IS, the PEG-nTiO_2 nanoparticles have more negative zeta potentials in the presence of cellulase than in the absence of cellulase. This significant decrease in the zeta potentials can be attributed to the adsorption of cellulase onto the PEG-nTiO_2 nanoparticles (*A. niger* cellulase is negatively charged at pH 5.5). This influence of adsorbed macromolecules such as NOM and proteins on the surface charge of nanoparticles has also been observed in other studies.[56-58]

At lower salt concentrations (3–100 mM NaCl), in the presence of cellulase, smaller hydrodynamic sizes were obtained compared to the size in the absence of cellulase. This can be attributed to stabilization of the nanoparticles by the cellulase molecules adsorbed on the particle surface. However, at higher salt concentrations, the particles have comparable zeta potentials in the presence and absence of cellulase resulting in similar hydrodynamic sizes. This may be due to a combination of factors including denaturing of cellulase that occurs at these high salt concentrations,[59] compression of the electrical double layer at the cellulase-coated particle surface, and/or compression of the enzyme molecule thereby eliminating any steric stabilizing effect of adsorbed cellulase.

TEM imaging of the PEG-nTiO_2 nanoparticles (Figure 2a) shows that the particles are polydisperse and mainly spherical. The diameter of each of the 350 particles was determined from the TEM images as analyzed by ImageJ software. The size distribution of the 350 nanoparticles is shown in Figure 2b with the sample studied consisting mostly of small particles (~ 30 nm) and few aggregates between 50 and 100 nm in size. DLS size measurements are significantly different from the size obtained by TEM

because they are strongly influenced by the presence of aggregates (the scattering intensity of the particles is roughly proportional to d^6).

3.2 Pre-coating the silica surface with cellulase

Flowing a suspension of cellulase (in NaCl solution) across the silica-coated crystal resulted in sharp frequency shifts (Δf) indicative of a fast deposition of cellulase onto the silica surface (Figure S2). The energy dissipation shifts (ΔD) obtained indicated the formation of a rigid layer of cellulase on the silica surface; namely, the ratio $-\Delta \boldsymbol{D}_{(3)}/\Delta \boldsymbol{f}_{(3)}$ for the cellulase film on silica was less than the empirical limit, suggested by the manufacturer of QCM-D (Q-Sense)[60], of 1×10^{-7} for a rigid film at all IS tested (Table S1). Upon rinsing the formed cellulase layer with the background artificial porewater, a stable baseline was obtained indicating that the cellulase film is firmly bound to the crystal surface. Representative measurements of the frequency and energy dissipation shifts obtained during the pre-coating of silica surface with cellulase are presented in Figure S3.

3.3 PEG-nTiO_2 deposition on bare and cellulase-coated silica

The deposition rates of PEG-nTiO_2 onto bare silica over a range of NaCl concentrations are presented in Figure 3a. Representative frequency shift measurements obtained during the deposition of PEG-nTiO_2 on bare and cellulase-coated silica are presented in Figure S4 and Figure S5. At low salt concentrations (10 – 60 mM NaCl), in the absence of cellulase, repulsive electrostatic interactions dominate between the negatively charged PEG-nTiO_2 and the negatively charged bare silica surface, resulting in unfavourable deposition of PEG-nTiO_2 under these conditions. This is consistent with behaviour observed in other deposition studies with fullerene, TiO_2, silicon nanocrystals (Si-NCs), quantum dots and CeO_2 nanoparticles in which unfavourable deposition conditions were observed at low IS.[8, 43, 49, 61-63]As IS increases, the degree of charge screening and double layer compression of the nanoparticles and silica surface increases resulting in higher deposition kinetics due to reduced repulsive forces. This is also consistent with previous studies in which increase in deposition rates was observed with increase in IS for unfavourable deposition conditions.[8, 11, 12, 64, 65] Also, changes in the energy dissipated with time (Figure 3b) can be used to determine the rate of particle deposition as the deposition of each particle yields an energy loss which is reflected in D.[43, 66] Comparison of Figures 3a and 3b shows similar trends in $d\Delta f_3/dt$ and $d\Delta D_3/dt$.

Deposition rates of PEG-nTiO_2 onto cellulase-coated silica over a range of NaCl concentrations are also presented in Figure 3a. These experiments show that interactions between the PEG-nTiO_2 and the cellulase-coated silica play a significant role in the particle deposition behaviour. In the absence of free cellulase in the solution, the deposition rate of PEG-TiO_2 onto cellulase-coated silica is significantly lower than that on bare silica. Similar trend was obtained in the measurements of $d\Delta D_3/dt$ (Figure 3b). The layer of cellulase molecules formed on the silica surface hindered the deposition of

PEG-nTiO_2 likely via electrosteric repulsion. Although it is not straightforward to compare the effect of the cellulase protein with that of a very differently structured organic macromolecule, this result is qualitatively in agreement with a previous study in which deposition of fullerene nanoparticles (NaCl, pH 5.5) onto humic acid-coated and alginate-coated silica surfaces resulted in significantly lower deposition rates (up to 1 order of magnitude) due to steric repulsion compared to deposition onto bare silica surface.[8] Also, a similar trend was observed in a study on the deposition of zinc oxide nanoparticles onto Suwannee River humic acid-coated silica surface.[67]

The ratio $-\Delta D_{(3)}/\Delta f_{(3)}$ provides insight into the rigidity of the deposited layer of particles and was calculated for each experimental condition (Figure 4). The calculated $-\Delta D_{(3)}/\Delta f_{(3)}$ ratios indicate that slightly viscoelastic nanoparticle films are formed on the bare silica at all IS (*i.e.*, $-\Delta D_{(3)}/\Delta f_{(3)} > 10^{-7}$). This is consistent with other studies in which polyacrylic-acid coated quantum dots and silicon nanocrystals capped with organic acids of varying alkyl-chain length formed viscoelastic layers.[51, 61]The nanoparticle films on the cellulase-coated silica are also mostly viscoelastic (Figure 4), and, in general, more so than the films formed on the bare silica (except at 10 mM NaCl). The behaviour of PEG-nTiO_2 observed at 10 mM NaCl can be attributed to the cellulase molecules on the silica surface. At 10 mM NaCl, as the particles approach the cellulase film, changes in the conformation of the cellulase molecules in the soft film creates a larger contact area for particle attachment. This results in a more rigid attachment of the particles onto the cellulase-coated silica compared to the bare silica at this low IS. This is qualitatively in agreement with a study by Olsson et al. in which it was determined that the presence of ligand-receptor interactions develops softer interfaces that yield stiffer bonds due to increased contact areas.[68] Olsson et al. suggest that a soft biotinylated polyethylene glycol (PEG) layer deposited onto a silica surface was deformed upon approach of silica particles thereby creating a larger contact area upon adhesion of the particles as compared to that of the bare silica surface thus yielding a more rigid attachment of the silica particles. As IS increases up to 100 mM NaCl, values of the $-\Delta D_{(3)}/\Delta f_{(3)}$ ratio tend to increase for deposition onto the cellulase-coated silica indicative of the formation of a more viscoelastic film of nanoparticles compared to films deposited on the bare silica. This suggests a change in the conformation of the cellulase molecules which makes the layer of cellulase molecules "less soft". Neutral salts such as NaCl can significantly impact the conformational stability of macromolecules such as cellulase due to the effect on the hydrophobic side chains on the interior of proteins.[69-71] Salts have been shown to induce a change in the solvent structure of the proteins thereby altering the thermodynamic equilibrium of the folded native structure of the protein.[69] Thus, the PEG-nTiO_2 particles deposit with a less stiff bond at this IS range compared to the lower IS. At the highest IS of 300 mM NaCl, it is likely that denaturing of the protein leads to a collapse of the cellulase molecules.[72] This results in a more rigid binding of the particles to the cellulase-coated surface at the highest IS tested. The relatively large ΔD_3 values indicate that the Sauerbrey equation (eq. 2) would underestimate the mass of deposited particles from the Δf_3 measurements. Thus, for the

purposes of this study, the particle deposition rates are reported in terms of the initial slope of the frequency shift as a function of time.

3.4 PEG-nTiO$_2$ deposition on cellulase-coated silica in the presence of suspended cellulase

A third series of experiments was conducted whereby the system was made more complex by addition of free cellulase in the background porewater solution used to suspend PEG-nTiO$_2$. Preliminary experiments were conducted to establish the extent of deposition of the suspended cellulase onto a silica surface pre-coated with cellulase in the absence of nanoparticles over a range of IS. Depending on the salt concentration, frequency shifts ranging from 2 to 4 Hz were observed when a 1 mL suspension of cellulase molecules (150 ppm) was introduced into the QCM-D chamber. These control experiments indicate little adsorption of free cellulase onto the layer of cellulase already formed on the silica surface. Therefore, in calculating the initial deposition rates of PEG-nTiO$_2$ in the presence of free (suspended) and pre-adsorbed cellulase, the Δf_3 contribution associated with deposition of cellulase at each IS was accounted for by subtracting the respective Δf_3 values. Attempts to quantify the amount of cellulase adsorbed onto the PEG-nTiO$_2$ particles using a colorimetric protein assay were unsuccessful.

Nanoparticle deposition experiments were performed by introducing a suspension of PEG-nTiO$_2$ + free cellulase into the chamber holding a cellulase-coated silica crystal. In these experiments, the PEG-nTiO$_2$ particle deposition rate was lower than that measured on both bare and cellulase-coated silica in the absence of free cellulase (Figures 3a and 3b). This is most likely due to improved electrosteric stabilization of PEG-nTiO$_2$ as a result of adsorption of cellulase onto the PEG-nTiO$_2$ surface and interaction of these coated particles with the adsorbed cellulase layer on the silica surface. This is consistent with the trend observed in a study on the deposition of fullerene nanoparticles in the presence of background humic acid on humic acid-coated silica surface in which it was observed that adsorption of humic acid on the fullerene nanoparticles resulted in a greater steric stabilization on top of the humic acid layer on the silica surface yielding a decrease in attachment efficiency.[8] This is also consistent with the zeta potential measurements whereby the nanoparticles are more negatively charged in the presence of free cellulase (Figure 1).

Calculated $-\Delta D_{(3)}/\Delta f_{(3)}$ ratios for experiments conducted with cellulase in suspension are the same as those measured in the absence of free cellulase onto cellulase-coated silica (Figure 4). This suggests that although fewer particles are deposited onto the cellulase-coated silica in the presence of free cellulase (Figure 3b), the viscoelasticity of the deposited PEG-nTiO$_2$ films on the cellulase-coated silica is the same both in the presence and absence of free cellulase and similar energy is dissipated upon deposition.

3.5 Measuring nanoparticle-surface interactions using an optical NanoTweezer

Figure 5 shows the interaction energy measurements that illustrate the extent of repulsion the particles experience when approaching the bare or cellulase-coated silica surface as a function of separation distance between the particle and the surface. The repulsive energy increases exponentially as the particle gets closer to the silica surface. In Figure 5a, for the bare silica surface, it can be observed that the extent of repulsion decreases with increasing salt concentration (at a given separation distance). A similar trend is observed in Figure 5b for the cellulase-coated silica surface. Figures 5c, 5d, and 5e, show a comparison of measurements carried out with bare and cellulase-coated silica at a given IS. The general trend observed is that the PEG-nTiO_2 particles encounter a lower repulsive energy when they approach the bare silica compared to the cellulase-coated silica (at a given separation distance).

Eq. 4 describes the interaction energy curves shown in Figure 5, and the values for A, a parameter related to steric and electrostatic interactions, and λ_D, the Debye length, can be determined by fitting the experimental data. The laser power necessary to trap PEG-nTiO_2 particles interacting with a bare or cellulase-coated silica surface and the corresponding calculated parameters that describe the potential energy maps are shown in Table 1.

Results shown in Table 1 for the calculated λ_D show that there is no statistically significant difference in Debye screening when comparing bare and cellulase-coated silica for the three IS tested. Nonetheless, we note a trend whereby λ_D values are larger for the cellulase-coated surface, implying that the particles start to interact with the coated surfaces at greater distances. In addition, it can be observed that the calculated A is statistically larger when the particle is interacting with a cellulase-coated silica, when comparing measurements obtained at the same IS. A is a parameter related to the steric and electrostatic interactions hence, this indicates that greater repulsive forces are present when the silica is coated with cellulase. The combination of both effects (higher electrosteric repulsion forces and similar Debye lengths) will result in the particle being repelled to a greater extent upon approach to the cellulase-coated surface than the bare surface. The NanoTweezer measurements complement the QCM-D experiments as they were conducted at lower IS (where QCM-D could not detect deposition) and therefore contribute to understanding the interactions between the particles and the surface over a wider range of conditions. The trends in the NanoTweezer measurements support the observations made in the QCM-D deposition experiments whereby more favourable interaction is observed with the bare silica than the cellulase-coated silica.

4. Conclusion

QCM-D was used to investigate the effect of cellulase on the deposition of PEG-nTiO_2 onto silica surfaces. The presence of cellulase whether pre-coated onto the silica surface or suspended in the background porewater solution resulted in significant reduction in deposition rates indicative of strong repulsive interactions between the particles and the layer of cellulase adsorbed on the silica surface. At all conditions examined, there was an increase in deposition rates with increase in solution IS due to weaker repulsive particle-surface electrostatic interactions with increasing salt concentration. Ratios of the dissipation shift to the frequency shift also gave insight into the rigidity of the deposited films. Except at the lowest IS studied (10 mM NaCl), more viscoelastic films were formed in the presence of cellulase compared to the films deposited on bare silica.

In many subsurface environments, extracellular soil enzymes may be present in the porewater as well as on the surface of soil or aquifer grains and suspended particles. The results of this study suggest that the presence of proteins such as extracellular cellulase may hinder the aggregation and deposition of ENPs thereby impacting their mobility in natural environments. Thus, the impact of extracellular soil proteins should be considered alongside other organic macromolecules such as humic and fulvic acids in the study of the fate and behaviour of ENPs.

Conflicts of interest

The authors declare that no competing financial interests exist.

Acknowledgements

This work was supported by the Nigerian Universities Commission (NUC), Presidential Special Scholarship for Innovation and Development (PRESSID, Nigeria), McGill University by a MEDA award to LMH, the Natural Sciences and Engineering Research Council of Canada (NSERC), the Canada Foundation for Innovation, and the Canada Research Chairs program. The authors thank A. Olsson for helpful discussions.

References

1. N. C. Mueller and B. Nowack, Exposure modeling of engineered nanoparticles in the environment, *Environmental Science & Technology*, 2008, **42**, 4447-4453.
2. W. J. Tseng and K.-C. Lin, Rheology and colloidal structure of aqueous TiO_2 nanoparticle suspensions, *Materials Science and Engineering: A*, 2003, **355**, 186-192.
3. R. Benedix, F. Dehn, J. Quaas and M. Orgass, Application of titanium dioxide photocatalysis to create self-cleaning building materials, *Lacer*, 2000, **5**, 157-168.
4. F. Gottschalk, T. Sonderer, R. W. Scholz and B. Nowack, Modeled environmental concentrations of engineered nanomaterials (TiO_2, ZnO, Ag, CNT, fullerenes) for different regions, *Environmental Science & Technology*, 2009, **43**, 9216-9222.
5. R. Kaegi, A. Ulrich, B. Sinnet, R. Vonbank, A. Wichser, S. Zuleeg, H. Simmler, S. Brunner, H. Vonmont and M. Burkhardt, Synthetic TiO_2 nanoparticle emission from exterior facades into the aquatic environment, *Environmental Pollution*, 2008, **156**, 233-239.
6. A. R. Petosa, S. J. Brennan, F. Rajput and N. Tufenkji, Transport of two metal oxide nanoparticles in saturated granular porous media: Role of water chemistry and particle coating, *Water Research*, 2012, **46**, 1273-1285.
7. A. R. Petosa, C. Öhl, F. Rajput and N. Tufenkji, Mobility of nanosized cerium dioxide and polymeric capsules in quartz and loamy sands saturated with model and natural groundwaters, *Water Research*, 2013, **47**, 5889-5900.
8. K. L. Chen and M. Elimelech, Interaction of fullerene (C60) nanoparticles with humic acid and alginate coated silica surfaces: measurements, mechanisms, and environmental implications, *Environmental Science & Technology*, 2008, **42**, 7607-7614.
9. C. Levard, E. M. Hotze, G. V. Lowry and G. E. Brown Jr, Environmental transformations of silver nanoparticles: impact on stability and toxicity, *Environmental Science & Technology*, 2012, **46**, 6900-6914.
10. M. Wiesner and J.-Y. Bottero, Environmental Nanotechnology: Applications and Impacts of Nanomaterials, McGraw-Hill Education, 2015.
11. A. R. Petosa, D. P. Jaisi, I. R. Quevedo, M. Elimelech and N. Tufenkji, Aggregation and Deposition of Engineered Nanomaterials in Aquatic Environments: Role of Physicochemical Interactions, *Environmental Science & Technology*, 2010, **44**, 6532-6549.
12. O. S. Alimi, J. Farner Budarz, L. M. Hernandez and N. Tufenkji, Microplastics and Nanoplastics in Aquatic Environments: Aggregation, Deposition, and Enhanced Contaminant Transport, *Environmental Science & Technology*, 2018, **52**, 1704-1724.
13. S. J. Klaine, P. J. Alvarez, G. E. Batley, T. F. Fernandes, R. D. Handy, D. Y. Lyon, S. Mahendra, M. J. McLaughlin and J. R. Lead, Nanomaterials in the environment: behavior,

fate, bioavailability, and effects, *Environmental Toxicology and Chemistry*, 2008, **27**, 1825-1851.

14. R. Kretzschmar, M. Borkovec, D. Grolimund and M. Elimelech, Mobile subsurface colloids and their role in contaminant transport, *Advances in Agronomy*, 1999, **66**, 121-193.
15. B. J. R. Thio, D. Zhou and A. A. Keller, Influence of natural organic matter on the aggregation and deposition of titanium dioxide nanoparticles, *Journal of Hazardous Materials*, 2011, **189**, 556-563.
16. K. Yang, D. Lin and B. Xing, Interactions of humic acid with nanosized inorganic oxides, *Langmuir*, 2009, **25**, 3571-3576.
17. R. F. Domingos, N. Tufenkji and K. J. Wilkinson, Aggregation of titanium dioxide nanoparticles: role of a fulvic acid, *Environmental Science & Technology*, 2009, **43**, 1282-1286.
18. M. Erhayem and M. Sohn, Stability studies for titanium dioxide nanoparticles upon adsorption of Suwannee River humic and fulvic acids and natural organic matter, *Science of the Total Environment*, 2014, **468**, 249-257.
19. A. Praetorius, J. Labille, M. Scheringer, A. Thill, K. Hungerbühler and J.-Y. Bottero, Heteroaggregation of titanium dioxide nanoparticles with model natural colloids under environmentally relevant conditions, *Environmental Science & Technology*, 2014, **48**, 10690-10698.
20. R. F. Domingos, C. Peyrot and K. J. Wilkinson, Aggregation of titanium dioxide nanoparticles: role of calcium and phosphate, *Environmental Chemistry*, 2010, **7**, 61-66.
21. N. Her, G. Amy, D. McKnight, J. Sohn and Y. Yoon, Characterization of DOM as a function of MW by fluorescence EEM and HPLC-SEC using UVA, DOC, and fluorescence detection, *Water Research*, 2003, **37**, 4295-4303.
22. J. Lu, S. Sanchez, C. Hofacre, J. J. Maurer, B. G. Harmon and M. D. Lee, Evaluation of broiler litter with reference to the microbial composition as assessed by using 16S rRNA and functional gene markers, *Applied and Environmental Microbiology*, 2003, **69**, 901-908.
23. M. Alexander, Introduction to Soil Microbiology, John Wiley & Sons., 1977
24. J. Skujiņš and R. Burns, Extracellular enzymes in soil, *CRC Critical Reviews in Microbiology*, 1976, **4**, 383-421.
25. S. D. Allison, T. B. Gartner, K. Holland, M. Weintraub and R. L. Sinsabaugh, Soil enzymes: linking proteomics and ecological processes in *Manual of Environmental Microbiology*, Third Edition, American Society of Microbiology, 2007, pp. 704-711.
26. K. Ikuma, Z. W. Shi, A. V. Walker and B. L. T. Lau, Effects of protein species and surface physicochemical features on the deposition of nanoparticles onto protein-coated planar surfaces, *RSC Advances*, 2016, **6**, 75491-75498.
27. S. Dominguez-Medina, J. Blankenburg, J. Olson, C. F. Landes and S. Link, Adsorption of a Protein Monolayer via Hydrophobic Interactions Prevents Nanoparticle Aggregation under

Harsh Environmental Conditions, *ACS Sustainable Chemistry & Engineering*, 2013, **1**, 833-842.

28. J. S. Gebauer, M. Malissek, S. Simon, S. K. Knauer, M. Maskos, R. H. Stauber, W. Peukert and L. Treuel, Impact of the Nanoparticle–Protein Corona on Colloidal Stability and Protein Structure, *Langmuir*, 2012, **28**, 9673-9679.
29. A. O. Luby, E. K. Breitner and K. K. Comfort, Preliminary protein corona formation stabilizes gold nanoparticles and improves deposition efficiency, *Applied Nanoscience*, 2016, **6**, 827-836.
30. M. Arianna, F. Ivana, T. Francesco and F. Bice, Interaction of fibrinogen and albumin with titanium dioxide nanoparticles of different crystalline phases, *Journal of Physics: Conference Series*, 2013, **429**, 012014.
31. M. Garvas, A. Testen, P. Umek, A. Gloter, T. Koklic and J. Strancar, Protein Corona Prevents TiO_2 Phototoxicity, *Plos One*, 2015.
32. T. Cedervall, I. Lynch, S. Lindman, T. Berggård, E. Thulin, H. Nilsson, K. Dawson and S. Linse, Understanding the nanoparticle-protein corona using methods to quantify exchange rates and affinities of proteins for nanoparticles, *Proceedings of the National Academy of Sciences*, 2007, **104**, 2050.
33. X. Xang, Y.P Zhang, Cellulases: Characteristics, Sources, Production, and Applications, in *Bioprocessing Technologies in Biorefinery for Sustainable Production of Fuels, Chemicals, and Polymers*, DOI: doi:10.1002/9781118642047.ch8.34.A. A. Safari Sinegani, *Factors affecting cellulase sorption in soil*, 2006.
34. A. A. Safari Sinegani, Factors affecting cellulase sorption in soil, *African Journal of Biotechnology* 2006, **5**, 467-471.
35. Y. Yopi, W. Tasia and R. Melliawati, Cellulase and Xylanase Production from Three Isolates of Indigenous Endophytic Fungi, 2017.
36. S. L. Hirsh, M. M. M. Bilek, N. J. Nosworthy, A. Kondyurin, C. G. dos Remedios and D. R. McKenzie, A Comparison of Covalent Immobilization and Physical Adsorption of a Cellulase Enzyme Mixture, *Langmuir*, 2010, **26**, 14380-14388.
37. A. A. Safari Sinegani, G. Emtiazi and H. Shariatmadari, Sorption and immobilization of cellulase on silicate clay minerals, *Journal of Colloid and Interface Science*, 2005, **290**, 39-44.
38. D. Zhang, H. E. Hegab, Y. Lvov, L. Dale Snow and J. Palmer, Immobilization of cellulase on a silica gel substrate modified using a 3-APTES self-assembled monolayer, *SpringerPlus*, 2016, **5**, 48.
39. W. Suvajittanont, M. K. Bothwell and J. McGuire, Adsorption of Trichoderma reesei CBHI cellulase on silanized silica, *Biotechnology and Bioengineering*, 2000, **69**, 688-692.
40. K. D. Mojsov, *Aspergillus Enzymes* for Food Industries in *New and Future Developments in Microbial Biotechnology and Bioengineering*, ed. V. K. Gupta, Elsevier, Amsterdam, 2016, DOI: https://doi.org/10.1016/B978-0-444-63505-1.00033-6, pp. 215-222.

41. D. B. Finkelstein, Improvement of enzyme production in Aspergillus, 1987.
42. R. Tedja, A. H. Soeriyadi, M. R. Whittaker, M. Lim, C. Marquis, C. Boyer, T. P. Davis and R. Amal, Effect of TiO_2 nanoparticle surface functionalization on protein adsorption, cellular uptake and cytotoxicity: the attachment of PEG comb polymers using catalytic chain transfer and thiol–ene chemistry, *Polymer Chemistry*, 2012, **3**, 2743-2751.
43. J. Fatisson, R. F. Domingos, K. J. Wilkinson and N. Tufenkji, Deposition of TiO_2 nanoparticles onto silica measured using a quartz crystal microbalance with dissipation monitoring, *Langmuir*, 2009, **25**, 6062-6069.
44. S. F. d. F. Alves PDD, Facchin S, Horta CCR, Victória JMN, Kalapothakis E., Survey of Microbial Enzymes in Soil, Water, and Plant Microenvironments, *The Open Microbiology Journal* 2014, **8**, 25–31.
45. L. Loperena, V. Soria, H. Varela, S. Lupo, A. Bergalli, M. Guigou, A. Pellegrino, A. Bernardo, A. Calviño, F. Rivas and S. Batista, Extracellular enzymes produced by microorganisms isolated from maritime Antarctica, *World Journal of Microbiology and Biotechnology*, 2012, **28**, 2249-2256.
46. R. J. Hunter, Foundations of Colloid Science, Oxford University Press, 2001.
47. G. Sauerbrey, Use of quartz vibration for weighing thin films on a microbalance, *Z. phys*, 1959, **155**, 206-212.
48. D. Johannsmann, I. Reviakine and R. P. Richter, Dissipation in films of adsorbed nanospheres studied by quartz crystal microbalance (QCM), *Analytical chemistry*, 2009, **81**, 8167-8176.
49. A. L. Olsson, I. R. Quevedo, D. He, M. Basnet and N. Tufenkji, Using the quartz crystal microbalance with dissipation monitoring to evaluate the size of nanoparticles deposited on surfaces, *ACS nano*, 2013, **7**, 7833-7843.
50. A. L. Olsson, A. Wargenau and N. Tufenkji, Optimizing Bacteriophage Surface Densities for Bacterial Capture and Sensing in Quartz Crystal Microbalance with Dissipation Monitoring, *ACS Applied Materials & Interfaces*, 2016, **8**, 13698-13706.
51. I. R. Quevedo, A. L. Olsson and N. Tufenkji, Deposition kinetics of quantum dots and polystyrene latex nanoparticles onto alumina: Role of water chemistry and particle coating, *Environmental Science & Technology*, 2013, **47**, 2212-2220.
52. P. Schein, C. K. Ashcroft, D. O'Dell, I. S. Adam, B. DiPaolo, M. Sabharwal, C. Shi, R. Hart, C. Earhart and D. Erickson, Near-Field Light Scattering Techniques for Measuring Nanoparticle-Surface Interaction Energies and Forces, *Journal of Lightwave Technology*, 2015, **33**, 3494-3502.
53. D. Erickson, X. Serey, Y.-F. Chen and S. Mandal, Nanomanipulation using near field photonics, *Lab on a Chip*, 2011, **11**, 995.
54. L. N. Ng, B. J. Luff, M. N. Zervas and J. S. Wilkinson, Propulsion of gold nanoparticles on optical waveguides, *Optics Communications*, 2002, **208**, 117-124.

55. M. Elimelech, J. Gregory and X. Jia, Particle deposition and aggregation: measurement, modelling and simulation, Butterworth-Heinemann, 2013.
56. K. L. Chen and M. Elimelech, Influence of humic acid on the aggregation kinetics of fullerene (C60) nanoparticles in monovalent and divalent electrolyte solutions, *Journal of Colloid and Interface Science*, 2007, **309**, 126-134.
57. M. M. Yallapu, N. Chauhan, S. F. Othman, V. Khalilzad-Sharghi, M. C. Ebeling, S. Khan, M. Jaggi and S. C. Chauhan, Implications of protein corona on physico-chemical and biological properties of magnetic nanoparticles, *Biomaterials*, 2015, **46**, 1-12.
58. J. Fatisson, I. R. Quevedo, K. J. Wilkinson and N. Tufenkji, Physicochemical characterization of engineered nanoparticles under physiological conditions: Effect of culture media components and particle surface coating, *Colloids and Surfaces B: Biointerfaces*, 2012, **91**, 198-204.
59. A. C. Dumetz, A. M. Snellinger-O'Brien, E. W. Kaler and A. M. Lenhoff, Patterns of protein–protein interactions in salt solutions and implications for protein crystallization, *Protein Science*, 2007, **16**, 1867-1877.
60. https://www.biolinscientific.com/qsense, (accessed July 5, 2018).
61. I. R. Quevedo, A. L. Olsson, R. J. Clark, J. G. Veinot and N. Tufenkji, Interpreting Deposition Behavior of Polydisperse Surface-Modified Nanoparticles Using QCM-D and Sand-Packed Columns, *Environmental Engineering Science*, 2014, **31**, 326-337.
62. K. L. Chen and M. Elimelech, Aggregation and deposition kinetics of fullerene (C60) nanoparticles, *Langmuir*, 2006, **22**, 10994-11001.
63. I. R. Quevedo and N. Tufenkji, Influence of solution chemistry on the deposition and detachment kinetics of a CdTe quantum dot examined using a quartz crystal microbalance, *Environ Science Technology*, 2009, **43**, 3176-3182.
64. A. J. Pelley and N. Tufenkji, Effect of particle size and natural organic matter on the migration of nano- and microscale latex particles in saturated porous media, *Journal of Colloid Interface Science*, 2008, **321**, 74-83.
65. B. Espinasse, E. M. Hotze and M. R. Wiesner, Transport and retention of colloidal aggregates of C60 in porous media: Effects of organic macromolecules, ionic composition, and preparation method, *Environmental Science & Technology*, 2007, **41**, 7396-7402
66. C. Poitras and N. Tufenkji, A QCM-D-based biosensor for E. coli O157:H7 highlighting the relevance of the dissipation slope as a transduction signal, *Biosensors and Bioelectronics*, 2009, **24**, 2137-2142.
67. X. Jiang, M. Tong, H. Li and K. Yang, Deposition kinetics of zinc oxide nanoparticles on natural organic matter coated silica surfaces, *Journal of Colloid and Interface Science*, 2010, **350**, 427-434.

68. A. L. Olsson, H. C. van der Mei, D. Johannsmann, H. J. Busscher and P. K. Sharma, Probing colloid–substratum contact stiffness by acoustic sensing in a liquid phase, *Analytical chemistry*, 2012, **84**, 4504-4512.
69. S. Damodaran and J. E. Kinsella, The effects of neutral salts on the stability of macromolecules. A new approach using a protein-ligand binding system, *Journal of Biological Chemistry*, 1981, **256**, 3394-3398.
70. T. Ohyashiki, M. Taka and T. Mohri, The effects of ionic strength on the protein conformation and the fluidity of porcine intestinal brush border membranes. Fluorometric studies using N-[7-dimethylamino-4-methylcoumarinyl]maleimide and pyrene, *Journal of Biological Chemistry*, 1985, **260**, 6857-6861.
71. M. V. Nguyen, K. A. Thorarinsdottir, A. Gudmundsdottir, G. Thorkelsson and S. Arason, The effects of salt concentration on conformational changes in cod (Gadus morhua) proteins during brine salting, *Food Chemistry*, 2011, **125**, 1013-1019.
72. S. Jacob, A. A. Shirwaikar, K. K. Srinivasan, A. Joseph, S. Lakshmana Prabu, M. Rathnanand and R. Kumar, Stability of proteins in aqueous solution and solid state, 2006.

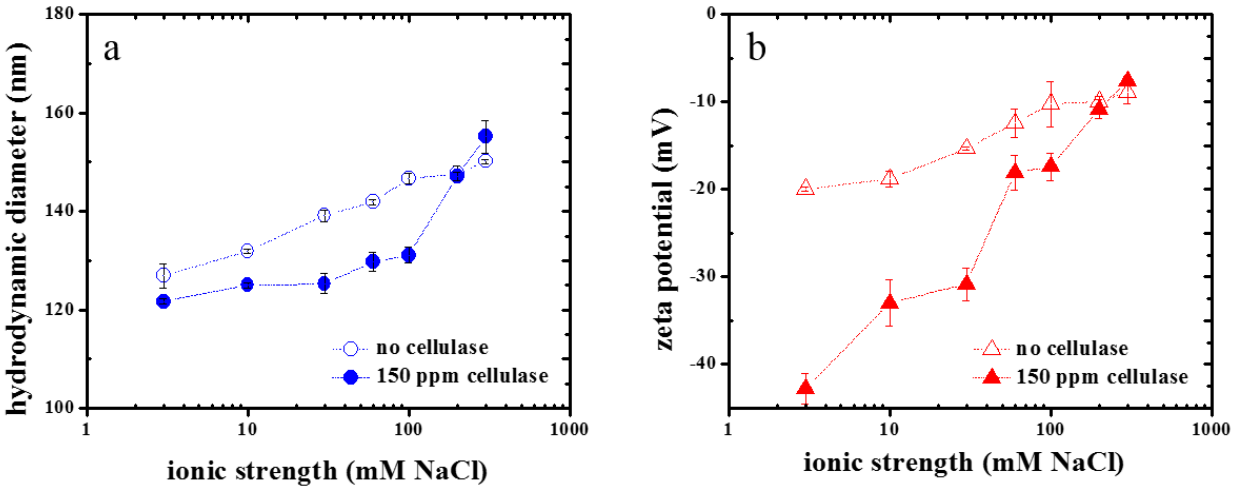

Figure 1. (a) Hydrodynamic diameter and (b) zeta potential of PEG-nTiO_2 as a function of salt concentration in the presence and absence of cellulase. Each data point represents the mean of at least triplicate measurements at the same experimental condition with error bars representing 95% confidence intervals. Dashed lines are included as eye guides only.

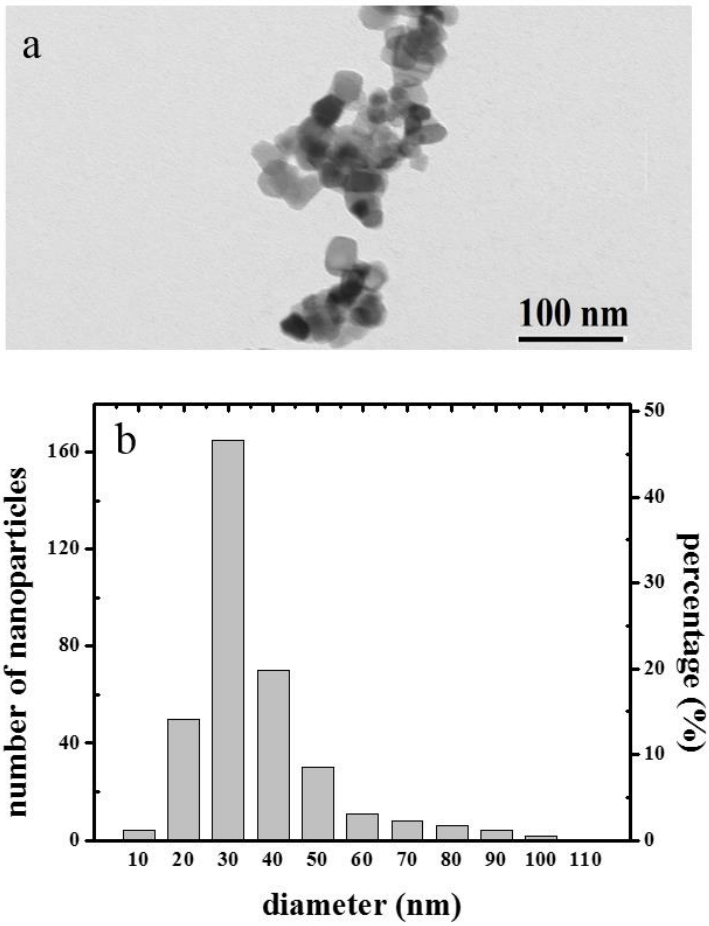

Figure 2. (a) TEM image of PEG-nTiO_2 nanoparticles and (b) size distribution of 350 PEG-nTiO_2 nanoparticles. Each bar represents a diameter range of 10 nm.

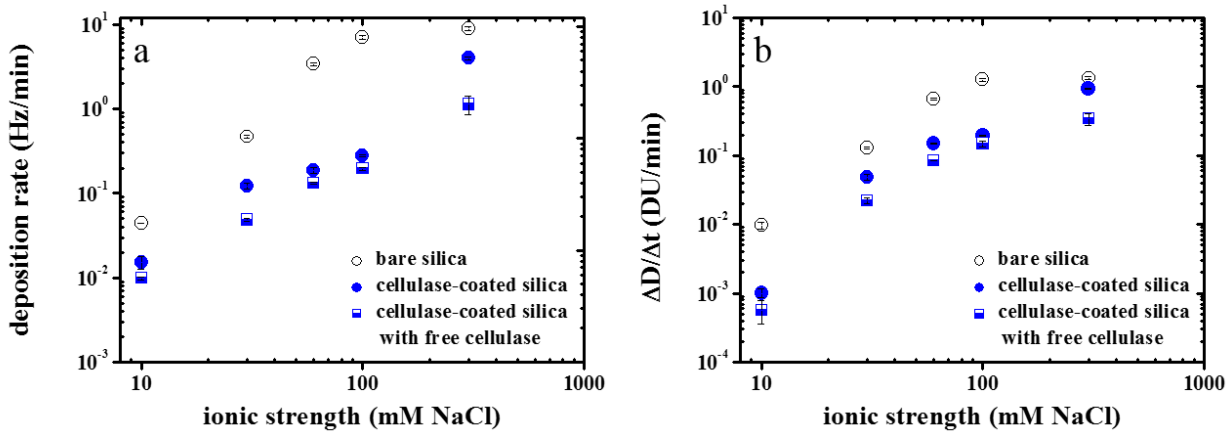

Figure 3. Average deposition rates determined from (a) $-d\Delta f_n/dt$ and (B) $d\Delta D_n/dt$ measurements for PEG-$nTiO_2$ suspended in NaCl at different salt concentrations (pH 5.5 ± 0.1) and different silica surface conditions determined from the 3rd overtone measurements. Each data point represents the mean of triplicate measurements at the same experimental condition with error bars representing 95% confidence interval.

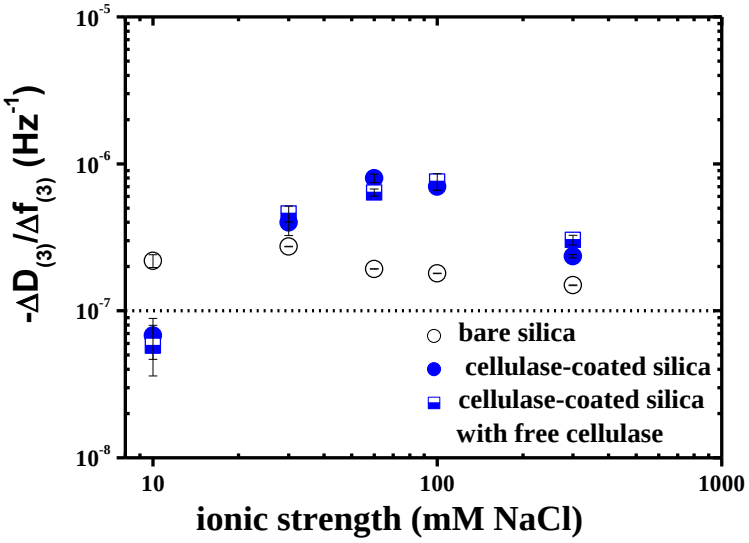

Figure 4. Ratio of $-\Delta D_{(3)}/\Delta f_{(3)}$ as a function of IS at all experimental conditions studied. The dotted line represents the limit of applicability for the Sauerbrey model as per Q-Sense.[34] Each data point represents the mean of triplicate measurements at the same experimental conditions with error bars representing 95% confidence interval.

(a) bare silica

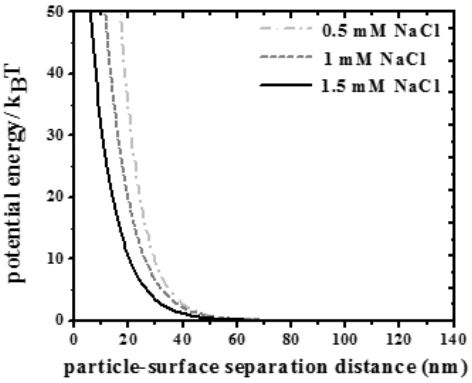

(b) cellulase-coated silica

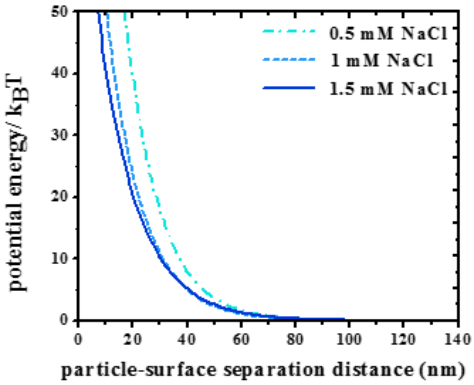

(c) 0.5 mM NaCl

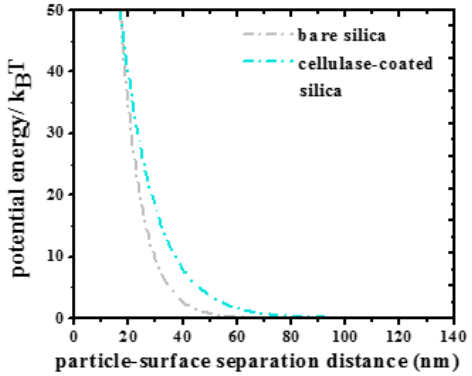

(d) 1.0 mM NaCl

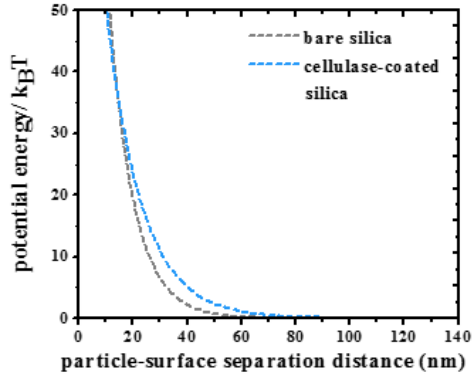

(e) 1.5 mM NaCl

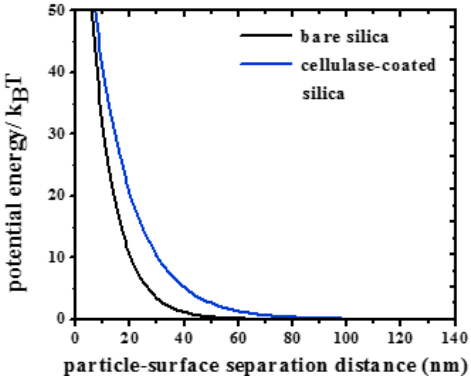

Figure 5. Interaction energy profiles for PEG-nTiO_2 interactions with (a) bare silica surface over an IS range of 0.5 – 1.5 mM NaCl, (b) cellulase-coated silica surface over an IS range of 0.5 – 1.5 mM NaCl, (c) bare and cellulase-coated silica surface at 0.5 mM NaCl, (d) bare and cellulase-coated silica surface at 1.0 mM NaCl (e) bare and cellulase-coated silica surface at 1.5 mM NaCl.

Table 1. Laser power required to trap particles at different conditions and calculated A and λ_D parameters

Silica surface treatment	Salt concentration (mM NaCl)	Laser power needed for particle capture (mV)	Calculated *A*	Calculated λ_D (Debye screening length) (nm)
bare silica	0.5	10	9.6 ± 0.8	7.9 ± 2.3
	1	10	6.6 ± 1.2	9.1 ± 2.2
	1.5	7	3.5 ± 0.7	9.1 ± 2.8
cellulase-coated silica	0.5	12.5	17.9 ± 1.1	12.6 ± 2.8
	1	11	11.0 ± 0.7	13.0 ± 2.0
	1.5	5.5	10.3 ± 1.2	14.6 ± 2.9